2011

The Synthesis and Characterization of Novel Ruthenium Terpyridine Complexes: Reactivity with DNA

Nicolette M. Jonkhoff
University of Redlands

THE SYNTHESIS AND CHARACTERIZATION OF NOVEL RUTHENIUM TERPYRIDINE COMPLEXES: REACTIVITY WITH DNA

by

Nicolette M. Jonkhoff

Honors thesis submitted to the Faculty of the University of Redlands
in partial fulfillment of the requirements for the degree of

BACHELOR OF SCIENCE

in

CHEMISTRY

Dr. J. Henry Acquaye, Advisor

Dr. Barbara Murray

Dr. David Schrum

Dr. Debra Van Engelen

Dr. Dan Wacks

May 28, 2011

Redlands, California

THE SYNTHESIS AND CHARACTERIZATION OF NOVEL RUTHENIUM TERPYRIDINE COMPLEXES: REACTIVITY WITH DNA

by

Nicolette M. Jonkhoff

(ABSTRACT)

Side effects associated with platinum-based anticancer therapies have resulted in the search for novel nonplatinum-based metal species. Among the different metal complexes generating interest, ruthenium complexes have shown great potential as anticancer agents. A series of mixed ligand ruthenium^{II} complexes with the formula *cis*-[Ru(X)(HPB)(OH_2)](PF_6), where X corresponds to either **(1)** Terpy = 2,2':6',2"-terpyridine; **(2)** Phterpy = 4'-Phenyl-2,2':6',2"-terpyridine or **(3)** Tterpy = 4'-Tolyl-2,2':6',2"-terpyridine, and HPB = 2-(2'-hydroxyphenyl)-benzoxazole, have been synthesized and structurally characterized. The DNA binding of the ruthenium^{II} complexes has been studied using several physical methods including absorption spectroscopy and competitive binding displacement assays. The ability of the complexes to unwind and / or untwist DNA has also been studied using supercoiled pUC18 DNA.

Table of Contents

List of Figures

List of Tables

List of Graphs

Acknowledgements

First and above all, I praise God, for providing me with the opportunity to study at the University of Redlands and granting me the capability to proceed successfully (Phillippians 4:13). This thesis appears in its current form due to the assistance and guidance of several people. I would therefore like to offer my sincere thanks to all of them.

Dr. Acquaye, my research advisor, for his never-ending enthusiasm, thoughtful guidance and critical comments through every stage of this project.

My thesis committee, for their valuable advice, patience and belief in me.

The Redlands science faculty for supporting undergraduate research, as well as the University of Redlands Summer Research Program for sponsoring my research over the past two summers.

For being sounding boards both inside and outside of lab I acknowledge Sean Currens, Phoebe Harpainter, Natasha Kozlyuk, Brandon Piasecki and Edgar Diaz Rosas. I am grateful as well for the genuine camaraderie that developed from spending four years with my peers in the Stauffer Science Complex.

And lastly I owe a debt of gratitude to my family. I could not have made it through this adventure without them.

1. Introduction

1.1. Inorganic chemistry

Active areas of research in inorganic chemistry include organometallic, coordination, biological and solid-state chemistry. Biological inorganic chemistry represents a burgeoning subdivision that has exploded into the scientific arena in recent years. Here the complementary nature of biology and chemistry is witnessed first-hand as both disciplines productively merge to tackle a variety of real-world problems. A cursory glance through the *Journal of Biological Inorganic Chemistry*, for instance, reveals both the applicability and comprehensiveness of active research projects within this domain.

1.2. Cisplatin

One such manifestation of the merger between the disciplines has been the development of cisplatin. Rosenberg and co-workers first reported its antitumor activity to *Nature* in 1969.[1] Known formally as *cis*–diamminedichloro platinum (II), this compound serendipitously went on to enter into the medical sector as a form of anticancer therapy in the 1970's. This intravenously administered agent induces cytotoxic effects mainly through its interaction with cellular DNA. Consequently it is often used to combat testicular, ovarian, head and neck cancer.[2] While derivatives have surfaced, including the second and third generation platinum-based drugs carboplatin and oxaliplatin, cisplatin continues to remain a widely used form of chemotherapeutic treatment today.

As its name implies, cisplatin is a platinum-based compound. Although platinum has two major valence states, +2 and +4, the square planar structures shown in **Figure 1** illustrate the +2 oxidation state.

Figure 1. Molecular structure of an active (*cis*– configuration) versus nonactive (*trans*– configuration) anticancer platinum complex. a) *cis*–diamminedichloro platinum (II) and b) *trans*–diamminedichloro platinum (II).

Molecular structural differences between *cis*– and *trans*– forms can help to explain why only the *cis*– configuration has active anticancer properties. In an effort to establish a causal relationship between structure and activity, Thompson and co-workers proposed several general characteristic traits.[3] From their work it has been proposed that active complexes: 1) may have either a square planar or octahedral geometry; 2) contain either two *cis*– monodentate leaving groups or one bidentate leaving group; 3) have a ligand exchange rate that is within an appropriate range; 4) are arranged such that leaving groups are roughly 3.4 angstroms apart on the molecule and /or 5) posses strongly bonded groups that are positioned across the molecule from the leaving group.

While a degree of ambiguity is still inherently present in efforts to differentiate conclusively between structure and activity, the proposed characteristics seem to present a reasonable argument as to why the *cis*– structure results in anticancer activity and the *trans*– structure does not.[4] Like many facets of science, however, exceptions to "the rule" do exist. Therefore the previously articulated structure-activity relationships should be interpreted loosely and in a fashion which recognizes the limits to its applications.

The proposed mechanism for chemotherapeutic action relies upon cisplatin's affinity for cellular DNA.[5,6,7] The anticancer agent is typically combined with a saline solution and, as mentioned previously, is administered in an intravenous fashion. Diffusion ushers the neutral

complex through the cell wall where, once inside, hydrolysis can occur - as depicted in **Figure 2.** This process enables the metal complex to become "activated", a key step necessary for interaction with the nucleophilic sites of DNA.[8]

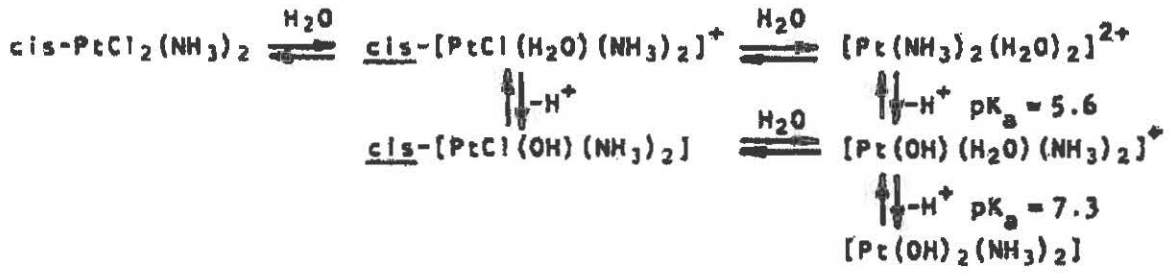

Figure 2. The hydrolysis of cisplatin inside the cell. $[Pt(OH)(H_2O)(NH_3)_2]^+$ is the most frequently occurring species under physiological conditions. Figure adopted from Reedijk and Lohman.[5]

The lability of the chloride ligands makes the complex susceptible to ligand substitution. Therefore as the chloride ligands become replaced step-wise with water molecules the complex gains an overall charge. This "activated" species can now interact via ligand substitution with a variety of biological nucleophiles. DNA, however, is believed to be the main target for cisplatin.[9]

Figure 3 represents four possible binding modes following the attack of cisplatin on DNA. Although the phosphate groups, sugar oxygen atoms and nucleobases of DNA all have electron lone pairs which could serve as binding sites for the metal complex, preference is given to the nucleobases.[10] Kinetic studies further suggest that the complex will first bind covalently to the purine base of DNA - notably N_7.[5] Adenine and guanine provide prime nucleophilic binding sites for the platinum drug and consequently the major bifunctional adduct formed is the intrastrand crosslink between N_7 atoms of two adjacent guanine residues.[11] This 1,2 intrastrand crosslink is not seen in DNA binding studies with transplatin due to sterics.

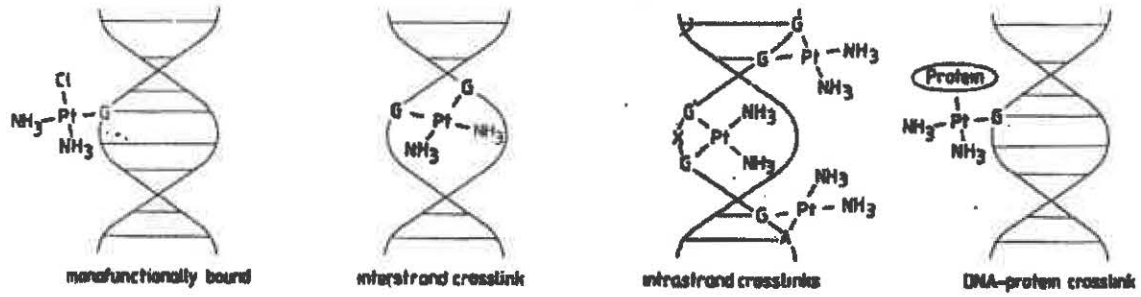

Figure 3. Several binding possibilities between cisplatin and DNA. The favored adduct form is the 1,2 intrastrand crosslink between two adjacent guanine (G) residues. Figure adopted from Reedijk and Lohman.[5]

Although cytotoxicity is an inherently complex process, the main molecular event that initiates this process is DNA damage. As expected, cisplatin's binding induces a major change in the DNA structure; not only do the bases become unstacked upon binding but, as highlighted in **Figure 4**, a kink in the DNA results.[6] From this point, DNA synthesis can become inhibited and RNA transcription can become suppressed.

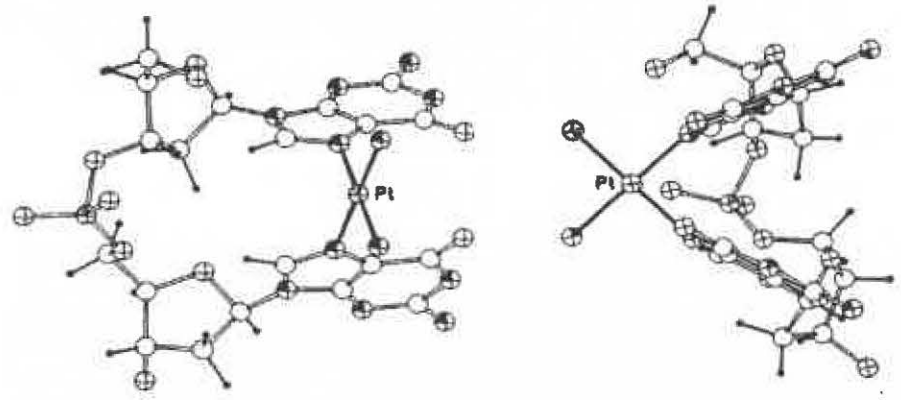

Figure 4. The binding of cisplatin to DNA induces a kink in the double helix. Figure adopted from Richards and Rodger.[6]

Although DNA modification is proposed to account for the drug's cytotoxic effects, it should be noted that cells do possess efficient repair systems. While some of the bifunctional lesions

induced by the drug may be repaired, it is unclear if cisplatin's toxic and mutagenic properties stem solely from lesions not able to be repaired in a timely manner.[5]

There is a fragile balance within oncology between the benefits of chemotherapy and correspondingly adverse side effects. Patients prescribed cisplatin are not immune to this teeter totter-like situation. And despite apparent effectiveness in the medical sector, it cannot be discounted that this platinum-based drug has been known to damage the kidneys, trigger hearing loss and induce nausea, vomiting and peripheral neurotoxicity.[12] Issues with regard to patients developing resistance to the drug have also surfaced in recent years.[13,14]

1.3. Ruthenium complexes

Detrimental toxicological effects have thus prompted researchers to search for alternatives to cisplatin, and interestingly ruthenium complexes have shown great potential as anticancer agents. A wide array of Ru^{II} and Ru^{III} complexes have been shown to exhibit cytotoxicity, including *mer*-[Ru^{III}(terpy)Cl_3] (where terpy = 2,2':6'2''-terpyridine)[15]; α-[Ru^{II}(azpy)$_2Cl_2$] (where azpy = 2-phenylazopyridine)[16] and organometallic complexes of the type [(η^6-arene)Ru^{II}(en)Cl]PF_6 (where en = ethylenediamine).[17]

Notably NAMI-A ([ImH][*trans*-$RuCl_4$(DMSO)(Im)], where Im = imidazole and DMSO = dimethyl sulfoxide) was the first ruthenium^{III} complex of its kind to enter into clinical trials in 1999 due in part to its good antimetastatic activity.[18] And in 2003, KP1019 ([IndH][*trans*-$RuCl_4(Ind)_2$], where Ind = indazole) was introduced into phase I clinical trials against colon carcinomas and their metastases.[19] (See **Figure 5**) Preliminary studies further suggest that some ruthenium complexes may be less toxic in comparison to their platinum-based counterparts.[20]

Such findings increase ruthenium's attractiveness to the medical sector and give merit to continue further study.

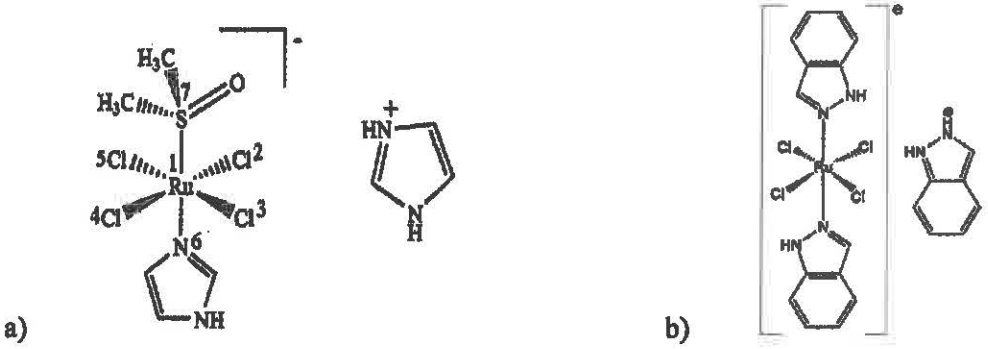

Figure 5. Structures of anticancer ruthenium complexes that have entered into clinical trials a) NAMI-A, ImH[*trans*-$RuCl_4$(DMSO)(Im)] and b) KP1019, [IndH][*trans*-$RuCl_4(Ind)_2$]. Structures adopted from Tan and co-workers.[21]

Ruthenium is a group eight transition metal that not only can access a broad range of oxidation states, 0 to +8, but can also occupy a wide array of coordination geometries.[22] While cisplatin and derivates may have a square planar arrangement, ruthenium complexes can often be found to have an octahedral, six-coordinated geometry. Activity of the ruthenium complex can thus be influenced by modifying the number and / or types of ligands bound to the transition metal center. Additionally, some ligands have been found to induce a degree of chirality to the complex.[15] Therefore in comparison to platinum-based complexes, ruthenium complexes have two additional binding sites which may allow for new binding modes to the target or even trigger a wider spectrum of activity.

In particular, ruthenium^{II} complexes containing polypyridyl chelating ligands have been studied extensively. Known to uniquely display rich photophysical and redox properties, multidentate polypyridyl ligands are often coupled to ruthenium complexes because they enhance DNA binding and photocleaving abilities.[23] Their applications, however, are not limited just to transition metals. The scope of polypyridyl complexes extends into the fields of

biochemistry, photochemistry and photophysics. Specifically these complexes have been employed to serve as photodynamic therapy (PDT) agents[24] and nucleic acid structural probes.[25]

Within the literature there is a reoccurring theme, notably with regard to the types of ligands studied. **Figure 6** highlights three frequently reported polypyridyl ligands that can be found coupled to ruthenium: 1,10-phenanthroline (phen); 2,2'-bipyridine (bpy) and dipyrido [3,2-a:2,',3'-c] phenazine (dppz). These ligands can form strong bonds to ruthenium mainly because they have vacant π orbitals that can accept electron density from the ruthenium ion.[26] This type of π backbonding enables the metal complex to have a relatively high degree of chemical stability.

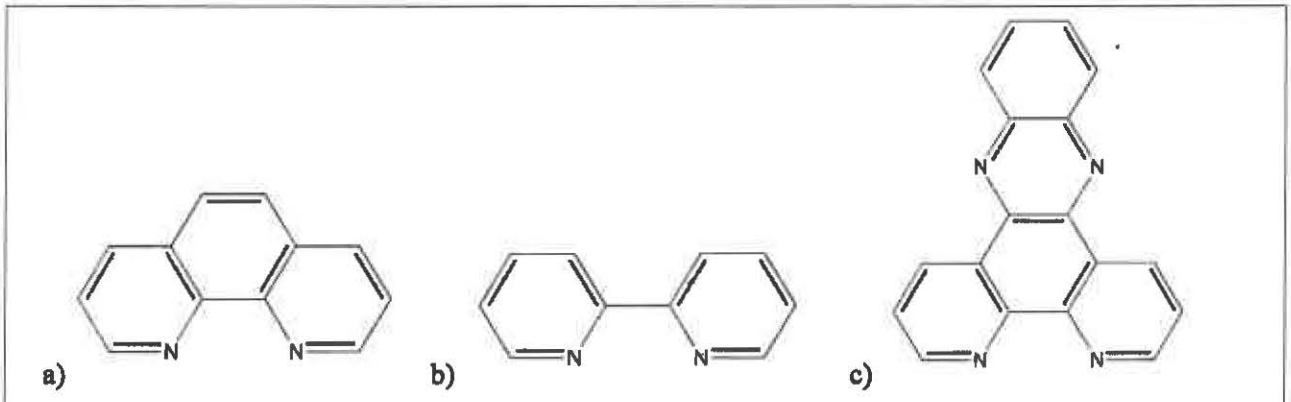

Figure 6. Frequently reported heterocyclic ligands that are often coupled to ruthenium a) phen; b) bpy and c) dppz.

Due in part to diverse DNA-binding modes, ruthenium^{II} complexes containing the bidentate polypyridyl ligand bpy have been found to be ideal DNA probes.[27] Under particular conditions some bpy complexes have also been reported to have efficient DNA photocleaving abilities.[28] Additionally, ruthenium complexes incorporating the dppz ligand have also been noted to bind to and photocleave DNA. Ambroise and Maiya, for instance, reported that the influence of the dppz ligand enabled their metal complex to exhibit interesting "electro-photo switch" effects.[29]

1.4. DNA binding

Ruthenium complexes containing polypyridyl ligands, as well as aqua or chloro groups, have been reported to bind to DNA.[30] In contrast to the stable pyridyl groups, aqua and chloro ligands are typically noted to be leaving ligands.[31]

Generally ruthenium^{II} complexes can bind to DNA with intercalating, groove binding and / or electrostatic binding modes. The mechanism of action for a metal complex to bind to DNA, however, is dependent both on the structure of the ruthenium complex and on the structure of the various ligands.[32] In order to deduce the mode, or strength, of action between the complex and the DNA, competitive binding displacement assays as well as cleavage gel assays, among others, can be carried out. It is useful as well to note that ruthenium polypyridyl complexes have good light absorbing properties. They can absorb throughout much of the ultraviolet and visible spectrum. Thus their light absorbing properties provide another useful way to monitor the interaction between the complex and DNA.

1.5. Current project

In this report the synthesis, characterization, electrochemical properties and DNA binding of a series of mixed ligand ruthenium^{II} complexes of the type *cis*-[Ru(X)(HPB)(OH_2)](PF_6), where X corresponds to either (**1**) Terpy = 2,2':6',2"-terpyridine; (**2**) Phterpy = 4'-Phenyl-2,2':6',2"-terpyridine or (**3**) Tterpy = 4'-Tolyl-2,2':6',2"-terpyridine, and HPB = 2-(2'-hydroxyphenyl)-benzoxazole, are explored (**Figures 7** and **8**). By beginning with the basic terpyridine ligand and adding various electron donating substituents (such as a phenyl or tolyl group) we hope to assess how the overall chemistry of the ruthenium complex is affected.

The rationale behind the particular design of these complexes is that tridentate ligands such as terpyridine and its extended derivatives have been less studied in this application. DNA binding properties of these complexes have also yet to be studied extensively, although terpyridine is noted to be an intercalating ligand.[33] Additionally, these terpyridine ligands are attractive in that they have a planar aromatic system which projects away from the metal center; they are also freely available and relatively easy to synthesize.

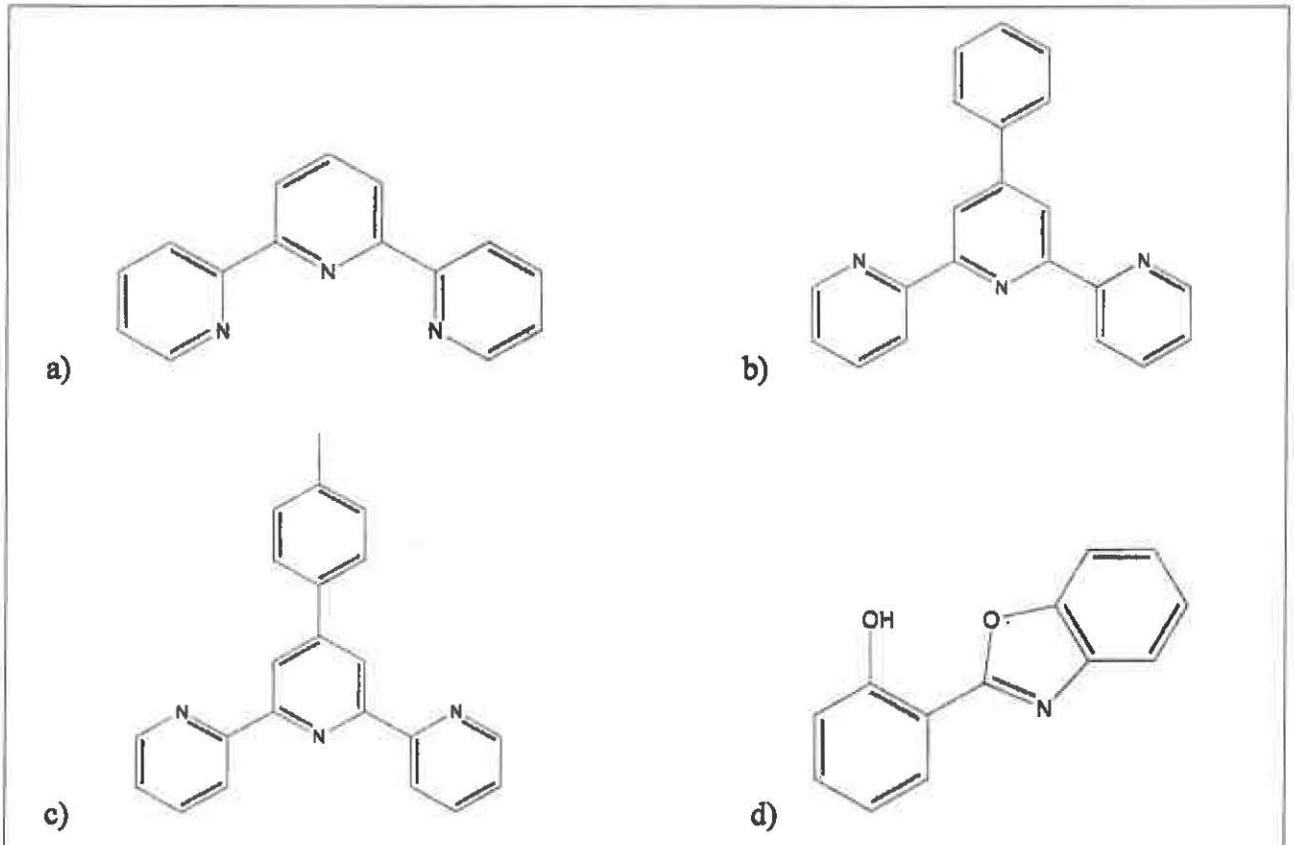

Figure 7. Ligands used in this report a) terpyridine (Terpy); b) phenyl terpyridine (Phterpy); c) tolyl terpyridine (Tterpy) and d) 2-(2'-hydroxyphenyl)-benzoxazole (HPB or ).
Various electron donating substituents (phenyl and tolyl group) were added to the basic terpyridine ligand in order to assess how the overall chemistry of the ruthenium complex was affected. Note that terpyridine is reported to be an intercalating ligand.[33]

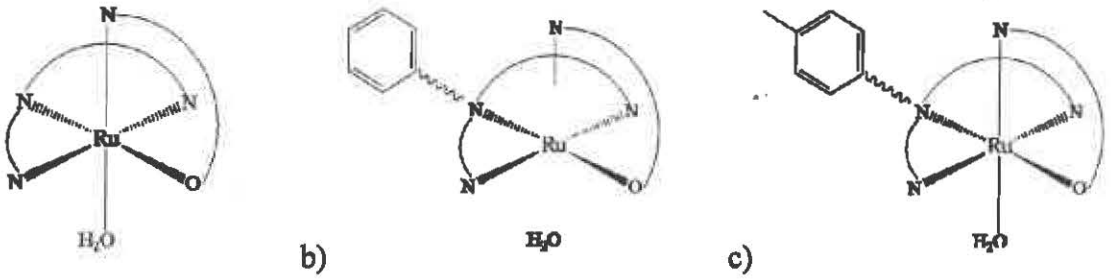

Figure 8. Three complexes synthesized in this report a) *cis*-[Ru(Terpy)(HPB)(OH_2)]; b) *cis*-[Ru(Phterpy)(HPB)(OH_2)] and c) *cis*-[Ru(Tterpy)(HPB)(OH_2)].

2. Experimental

2.1. Materials

All solvents and materials used for preparation were reagent grade, purchased from the Sigma Aldrich Company (St. Louis, MO) and used as received without further purification. Calf thymus (CT) DNA and plasmid DNA (pUC18) were also purchased from Sigma Aldrich.

2.2. Techniques and instrumentation

Deionized water was used to prepare all buffers. Phosphate buffer (pH 7.0) was prepared by dissolving sodium phosphate, NaH_2PO_4, (600 mg) in approximately 450 mL water. The solution was titrated to pH 7.04 with strong acid or base as needed and the final volume was made up to 500 mL. Tris base buffer (10 mM, pH 7.1) was prepared by dissolving Tris base (300 mg) in approximately 100 mL water. The solution was titrated to pH 7.1 with sulfuric acid and the final volume was made up to 150 mL.

A solution of CT-DNA was prepared by dissolving one frozen DNA pellet in a fresh solution of phosphate buffer (25 mL, pH 7.0). The DNA stock solution was not used for any reactivity studies until it was homogenous in composition. The freshly prepared solution was stored in the

refrigerator until needed and for optimal results the solution was typically used within five days. A plasmid DNA solution was prepared by diluting the frozen pUC18 DNA sample with Tris base buffer (20 μL) and was stored in the freezer until needed. A 1% stock solution of ethidium bromide (EB) (2.2536×10^{-2} M) was prepared and diluted as needed using deionized water.

Absorption measurements were recorded using a 1.0 cm quartz cuvette on a Shimadzu PharmSpec 1700 UV-Vis Spectrophotometer. A solution of CT-DNA in phosphate buffer (pH 7.0) gave a ratio of UV absorbance at 260 and 280 nm of about 1.8-1.9, indicating that the DNA was sufficiently free of protein.[34] The concentration of CT-DNA was determined by using the molar absorption coefficient (6600 $M^{-1}cm^{-1}$) at 260 nm.[35]

UV-Vis spectra were recorded on a Jasco V-530 UV-Vis Spectrophotometer which was equipped with a thermostated Fisher Scientific Isotemp 3028 temperature control compartment. The reactions were recorded in a 1.0 cm quartz cell and analyzed using Spectra Manager software. The substitution of the aqua ligand was monitored by following the change in absorbance between 720-765 nm.

Cyclic voltammetry studies were performed in dichloromethane using a BAS CV-Solv voltammetric analyzer. A single compartment cell with a three electrode set-up was used which consisted of a platinum disk working electrode, platinum wire auxiliary electrode and an Ag/AgCl reference electrode. The platinum disk working electrode was polished using alumina before each use. The supporting electrolyte was tetrabutylammonium hexafluorophosphate, Bu_4NPF_6 (0.1 M). Samples were purged with nitrogen gas for two-three minutes before scans and scans were performed under a nitrogen gas atmosphere at room temperature. The scan rate for each measurement was 100 mV/s.

Fluorescence spectra were taken in 1.0 cm quartz cells and recorded using a Jasco FP-750 Spectrofluorometer.

pH measurements were performed using an Accumel pH meter which was calibrated using three pre-made standard buffer solutions (pH 4, 7 and 10).

Elemental analyses were performed by Galbraith Laboratories, Inc. (Knoxville, TN).

2.3. Syntheses[36]

2.3.1. $Ru(X)Cl_3$ (where X = Terpy; Phterpy; Tterpy)

A solution containing $RuCl_3 \cdot 3H_2O$ (540 mg) and 50 mL ethanol was degassed with nitrogen gas for five minutes. 2,2':6'2"-terpyridine (560 mg) was added and the solution was refluxed under nitrogen gas for four hours. The mixture was allowed to cool and the brick red precipitate was washed several times with ethanol until the washing was colorless. The product was dried under vacuum for one day. A similar procedure was used for the Phterpy and Tterpy complexes. Yield: 870 mg - 2120 mg.

$Ru(Terpy)Cl_3$ yield: 870 mg

$Ru(Phterpy)Cl_3$ yield: 900 mg

$Ru(Tterpy)Cl_3$ yield: 2.120 g

2.3.2. *cis*– and *trans*–[Ru(X)(HPB)Cl] (where X = Terpy; Phterpy; Tterpy)

$Ru(terpy)Cl_3$ (400 mg) was added to a mixture of ethanol and deionized water, 40 mL and 15 mL, respectively. The solution was degassed with nitrogen for five minutes. 2-(2'-hydroxyphenyl)-benzoxazole (200 mg) was dissolved in 15 mL hot ethanol and added to the ruthenium solution. Triethylamine, 1 mL, was added and the solution was refluxed under

nitrogen gas for four hours (**Figure 9**). After cooling, the solution was filtered and the product was washed with ethanol until the washing was colorless. The solid was then washed with 5 mL deionized water, followed by 10 mL ethanol and 10 mL ether. The solid product (*trans*–) was allowed to air dry. A similar procedure was used for the Phterpy and Tterpy complexes. Yield: 274 mg -700 mg.

trans–Ru(Terpy)(HBP)Cl yield: 274 mg

trans–Ru(Phterpy)(HBP)Cl yield: 300 mg

trans–Ru(Tterpy)(HBP)Cl yield: 700 mg

The filtrate was rotary evaporated to dryness. 20 mL deionized water was added and the mixture was sonicated for two minutes. The solution was filtered and washed several times with deionized water. The product (*cis*–) was allowed to air dry. A similar procedure was used for the Phterpy and Tterpy complexes. Yield: 78 mg - 233 mg.

cis –Ru(Terpy)(HBP)Cl yield: 233 mg

cis –Ru(Phterpy)(HBP)Cl yield: 100 mg

cis –Ru(Tterpy)(HBP)Cl yield: 78 mg

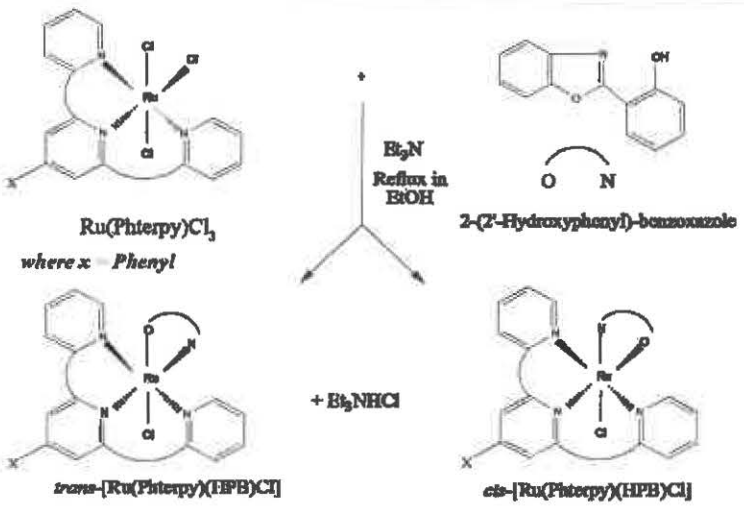

Figure 9. Synthesis of the Ru(Phterpy)(HPB)Cl isomers.

2.3.3. *cis*–[Ru(X)(HPB)(H_2O)](PF_6) (where X = Terpy(**1**); Phterpy(**2**); Tterpy(**3**))

cis–Ru(Terpy)(HPB)Cl (100 mg) was added to a mixture of deionized water and acetone, 30 mL and 20 mL, respectively. Silver hexafluorophosphate, $AgPF_6$, (130 mg) was added and the solution was refluxed under nitrogen gas for one hour. After cooling to room temperature, the solution was further cooled in an ice bath for a half hour. A fine glass frit was used to filter the solution. Ammonium hexafluorophosphate, NH_4PF_6, (1.0 g) was added to the filtrate and the solution was stored in the refrigerator overnight. The dark green microcrystals were then filtered with 5 mL cold deionized water. The product was allowed to air dry and was characterized to be complex **1**. A similar procedure was used for the Phterpy and Tterpy complexes, characterized to be complexes **2** and **3**, respectively. Elemental analysis data was recorded for complex **2**. Yield: 104 mg - 150 mg.

(1) *cis* –[Ru(Terpy)(HBP)(H_2O)](PF_6) yield: 104 mg

(2) *cis* –[Ru(Phterpy)(HBP)(H_2O)](PF_6) yield: 120 mg

(3) *cis* –[Ru(Tterpy)(HBP)(H_2O)](PF_6) yield: 150 mg

2.4. Characterization studies

2.4.1. UV-Vis

The UV-Vis spectra of the *cis*– and *trans*–Ru(X)(HPB)Cl complexes, as well as the *cis*– and *trans*–[Ru(X)(HPB)(H_2O)](PF_6) complexes, were recorded in dichloromethane between 235 and 900 nm.

2.4.2. Cyclic voltammetry

The electrochemical characteristics of complexes **1**, **2** and **3** were investigated using a cyclic voltammetry technique, as previously described in section 2.2.

2.4.3. Time-lapsed kinetics

Ruthenium complex **1** (6 mg) was dissolved in phosphate buffer (25 mL, pH 7.0). CT-DNA (0.75 mL) was added to the ruthenium solution (0.25 mL) and an absorption spectrum was recorded overnight in ninety minute intervals between 400-900 nm. The temperature was kept constant at 37 °C. A similar procedure was carried out for complexes **2** and **3**.

2.4.4. X-ray crystal structure determination

X-ray crystal structure determination was performed by Dr. Fook S. Tham at the Department of Chemistry, University of California, Riverside, CA. A black fragment of a prism (0.47 x 0.43 x 0.23 mm^3) was used for the single crystal x-ray diffraction study of $C_{34}H_{23}N_4O_2ClRu \cdot PF_6 \cdot [H_2O]_{1.21}$ (sample ha13_0m). The crystal was coated with paratone oil and mounted on to a cryo-loop glass fiber. X-ray intensity data were collected at 100(2) K on a Bruker APEX2

platform-CCD x-ray diffractometer system (Mo-radiation, λ = 0.71073 Å, 50KV/40mA power).[37] The CCD detector was placed at a distance of 5.0670 cm from the crystal.

A total of 3600 frames were collected for a sphere of reflections (with scan width of 0.3° in ω, starting ω and 2θ angles of –30°, and ϕ angles of 0°, 90°, 120°, 180°, 240°, and 270° for every 600 frames, 20 sec/frame exposure time). The frames were integrated using the Bruker SAINT software package and using a narrow-frame integration algorithm.[38] Based on a triclinic crystal system, the integrated frames yielded a total of 35319 reflections at a maximum 2θ angle of 59.14° (0.72 Å resolution), of which 8852 were independent reflections (R_{int} = 0.0153, R_{sig} = 0.0125, redundancy = 4.0, completeness = 99.7%) and 8459 (95.6%) reflections were greater than 2σ(I). The unit cell parameters were, a = 10.1967(3) Å, b = 11.9503(4) Å, c = 14.1934(5) Å, α = 112.8086(4)°, β = 91.7830(4)°, γ = 95.5838(4)°, V = 1582.24(9) Å^3, Z = 2, calculated density D_c = 1.727 g/cm^3. Absorption corrections were applied (absorption coefficient μ = 0.711 mm^{-1}; max/min transmission = 0.8541/0.7319) to the raw intensity data using the SADABS program.[39]

The Bruker SHELXTL software package was used for phase determination and structure refinement.[40] The distribution of intensities (E^2-1 = 0.853) and no systematic absent reflections indicated two possible space groups, P-1 and P1. The space group P-1 (#2) was later determined to be correct.. Direct methods of phase determination followed by two Fourier cycles of refinement led to an electron density map from which most of the non-hydrogen atoms were identified in the asymmetry unit of the unit cell. With subsequent isotropic refinement, all of the non-hydrogen atoms were identified. There was one cation of $C_{34}H_{23}N_4O_2ClRu$, one anion of PF_6, and 1.21 water molecules present in the asymmetry unit of the unit cell. The water molecules were hydrogen bonded to the oxygen, fluorine and chlorine atoms.

Atomic coordinates, isotropic and anisotropic displacement parameters of all the non-hydrogen atoms were refined by means of a full matrix least-squares procedure on F^2. The H-atoms were included in the refinement in calculated positions riding on the atoms to which they were attached, except the H-atoms involved in hydrogen bonding. The refinement converged at $R_1 = 0.0229$, $wR_2 = 0.0599$, with intensity, $I>2\sigma(I)$. The largest peak/hole in the final difference map was 1.569/-0.387 e/Å^3. The high electron density peak (1.569 e/Å^3) next to the Ru-atom was probably due to absorption corrections error. The crystallographic data are summarized in **Appendix 1** and the structured described is in **Figure 14.**

2.4.5. Absorption spectral study

Absorption titration of the ruthenium complex was performed by loosely following a procedure published by Gao and co-workers.[27] The concentrations of the CT-DNA and ruthenium solution were adjusted such that the DNA was about ten times more concentrated than the ruthenium solution. Keeping the ruthenium solution volume constant (0.2 mL, 7.61×10^{-5} M) and the total solution volume at 1 mL, increasing amounts of CT-DNA were added. Phosphate buffer (pH 7.0) was added as needed to keep the total volume of each trial constant. Complex-DNA solutions were incubated in a warm water bath at 37 °C for ten minutes prior to each UV-Vis scan between 400-900 nm. Phosphate buffer was used in the reference cell.

2.4.6. Competitive binding displacement with ethidium bromide (EB)

CT-DNA competitive binding experiments with EB were carried out in phosphate buffer (pH 7.0). As suggested by Tan and co-workers, the ratio of CT-DNA to EB was fixed for each trial ([CT-DNA]/[EB] = 5) and the concentration of the ruthenium complex was varied accordingly

([Ru] = 0-300 μM).[41] The components were mixed in a vial by repeated inversion upon addition of the ruthenium solution to a mixture of CT-DNA and EB. Solutions were allowed to sit at room temperature for twenty minutes before being analyzed by fluorometry. The excitation wavelength was 537 nm and the emission range was set between 500-700 nm.

The spectra were further analyzed using the Stern-Volmer equation (1), where I_0 and I are the fluorescence intensities in the absence and presence of the complexes, respectively, K_{sv} is the Stern-Volmer quenching constant, and r is the ratio of the total concentration of the complex to the CT-DNA ([Ru]/[CT-DNA]).

$$\frac{I_0}{I} = 1 + K_{sv}r \quad (1)$$

2.4.7. DNA cleavage

A slightly modified procedure published by Deshpande and co-workers was used to analyze the binding of the metal complexes to supercoiled pUC18 DNA via agarose gel electrophoresis.[42] Plasmid DNA (2 μL) was treated with different concentrations of the metal complex (0-10 μM) and the mixtures were incubated briefly for one hour in the dark at 37 °C. After incubation, the reactions were quenched by the addition of 6X loading dye (2 μL). The samples were then loaded into the wells and subjected to electrophoresis for ninety minutes at 60 V on 1.2 % agarose gel stained with EB in TAE buffer. The gel was visualized by UV light and photographed for analysis.

3. Results and discussion

3.1. Syntheses

Mixed ligand ruthenium^{II} complexes with the formula *cis*-[Ru(Terpy)(HPB)(OH_2)](PF_6) **1**, *cis*-[Ru(Phterpy)(HPB)(OH_2)](PF_6) **2** and *cis*-[Ru(Tterpy)(HPB)(OH_2)](PF_6) **3** have been synthesized.

Elemental analyses *cis*-[Ru(Phterpy)(HPB)(OH_2)](PF_6)$_2$·2H_2O [$RuC_{34}H_{25}N_4O_3P_2F_{12}$·2$H_2O$] calculated (found): C, 42.33 (42.05); H, 3.04 (3.09); N, 5.81 (5.71).

Elemental analyses *trans*-[Ru(Phterpy)(HPB)(OH_2)](PF_6)·2H_2O [$RuC_{34}H_{25}N_4O_3PF_6$·2H_2O] calculated (found): C, 49.81 (49.45); H, 3.08 (3.11); N, 6.84 (6.69).

3.2. Characterization

3.2.1. UV-Vis

In order to study the light absorbing properties of the ruthenium complexes, an electronic absorption spectrum was recorded for each metal complex in dichloromethane. Specifically it was of interest to note any changes between the absorption spectrum of the chloro complex and the absorption spectrum of the aqua complex, as this would be used to later help interpret data from reactions which combined the metal aqua complex with CT-DNA.

In order to properly assign each band to a particular transition it was necessary to consider the molecular orbital diagram for a d^6 octahedral metal complex (**Figure 10**). The most important orbitals in major electronic transitions to make note of are the filled metal π-orbital (HOMO) and the unfilled ligand π^*-orbital (LUMO).

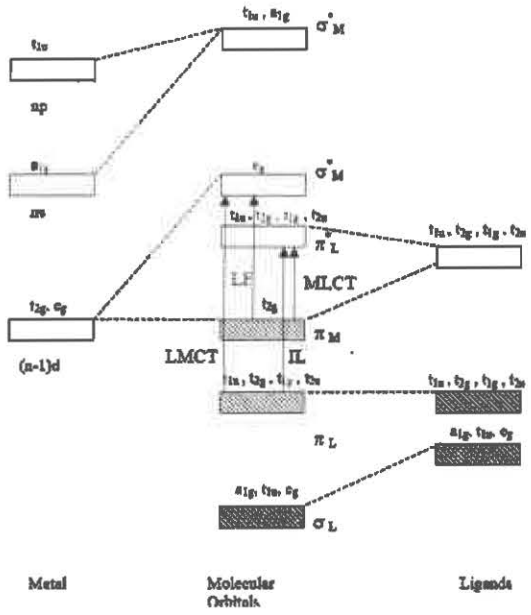

Figure 10. Molecular orbital diagram for a d^6 octahedral metal complex. Shaded boxes refer to a filled molecular orbital and arrows represent common transitions. MLCT= metal to ligand charge transfer; LMCT=ligand to metal charge transfer.

Table 1 highlights the electronic spectral data for the Phterpy complexes synthesized in this report. The electronic spectra for the two chloro isomers, Ru(Phterpy)(HPB)Cl, are similar, with only slight variations in the λ_{max}. Notably the chloro isomers feature two high energy transitions in the ultra violet region between 240-350 nm which likely correspond to the π-π^*transitions in both the Phterpy and HPB ligands.[43] It is difficult however to determine which ligand directly corresponds to which transition in this region. Nonetheless, these two bands were found to be present in the absorption spectrum of the aqua complexes as well. This is to be expected since both the chloro and aqua complexes contain the Phterpy and HPB ligands. The chloro complexes also feature two lower energy transitions in the visible region between 400 and 600 nm which can be attributed to a metal to ligand charge transfer (MLCT) from the d-orbital of the metal complex to the π^*-orbital of the Phterpy and HPB ligands.[44]

The appearance of a broad band in the visible region at about 750 nm was a striking feature evident only in the spectra for the two aqua isomers, [Ru(Phterpy)(HPB)(H_2O)](PF_6)$_2$ (**Figure 11**). The introduction of a broad band in the aqua complex spectrum was consistent with results obtained by Claustro and co-workers for similar terpyridine complexes.[36] As suggested by Balzani and co-workers, these bands likely correspond to ligand to metal charge transfers (LMCT).[45]

Table 1. Electronic spectral data

Complex	λ_{max} (log ε)
cis-Ru(Phterpy)(HPB)Cl	281 (4.69); 322 (4.26); 400 (4.11); 583 (3.94)
trans-Ru(Phterpy)(HPB)Cl	284 (4.61); 323 (4.4); 402 (4.11); 581 (3.88)
cis-[Ru(Phterpy)(HPB)(H_2O)](PF_6)$_2$ **(2)**	286 (4.52); 335 (4.37); 406 (3.84); 757 (3.64)
trans-[Ru(Phterpy)(HPB)(H_2O)](PF_6)	286 (5.33); 334 (5.04); 430 (4.48); 720 (4.36)

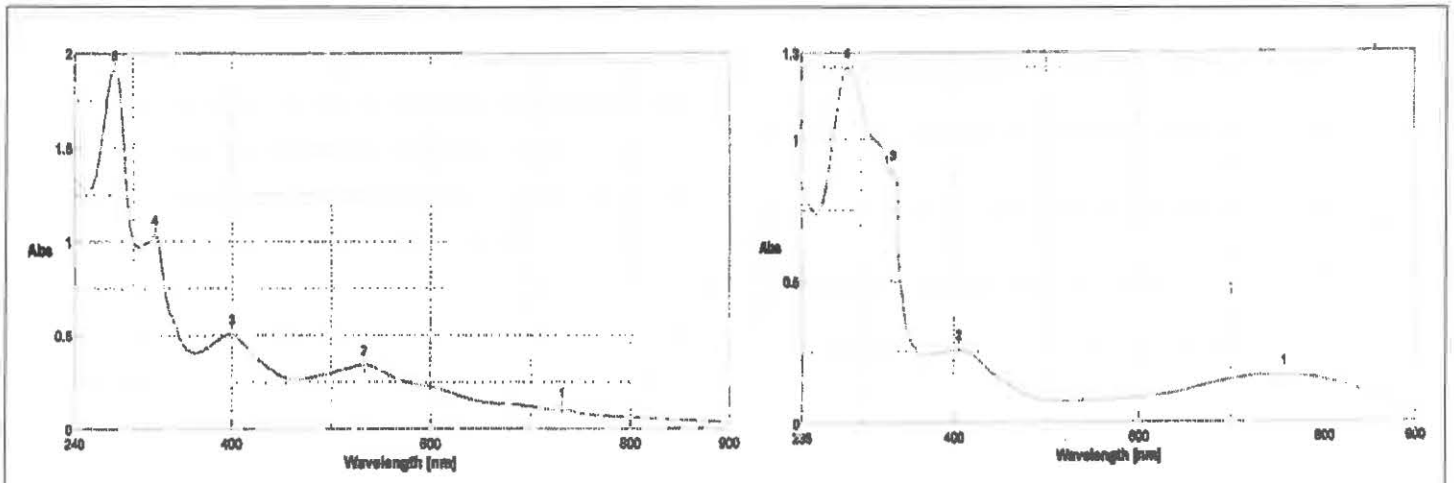

cis-Ru(Phterpy)(HPB)Cl

cis-[Ru(Phterpy)(HPB)(H_2O)](PF_6)$_2$ **(2)**

Figure 11. UV-Vis spectra of a chloro and aqua complex recorded in dichloromethane. The chloro complex (on the left) and the aqua complex (on the right) both have similar absorption bands between 200 and 500 nm. Note however that the chloro complex does not have an absorption band in the 750 nm region while the aqua complex does. In other words, substitution of the chloride ligand with an aqua ligand results in the appearance of a new peak around 750 nm.

3.2.2. Cyclic voltammetry

The electrochemical behavior of the complexes were studied in dichloromethane. **Table 2** highlights the results. The cyclic voltammograms show one distinct redox process occurring which suggests that the samples are pure (**Figure 12**). The corresponding $E_{1/2}$ for the reversible couple of *cis*-Ru(Phterpy)(HPB)Cl and *cis*-[Ru(Phterpy)(HPB)(H_2O)](PF_6)$_2$ are 293 mV and 494.5 mV, respectively. The corresponding $E_{1/2}$ for the reversible couple of *trans*-Ru(Phterpy)(HPB)Cl and *trans*-[Ru(Phterpy)(HPB)(H_2O)](PF_6)$_2$ are 171.2 mV and 163 mV, respectively.

Table 2. Electrochemical data

Complex	$E_{1/2}$ (mV)
cis-Ru(Phterpy)(HPB)Cl	293
trans-Ru(Phterpy)(HPB)Cl	171.5
cis-[Ru(Phterpy)(HPB)(H_2O)](PF_6)$_2$ **(2)**	494.5
trans-[Ru(Phterpy)(HPB)(H_2O)](PF_6)	163

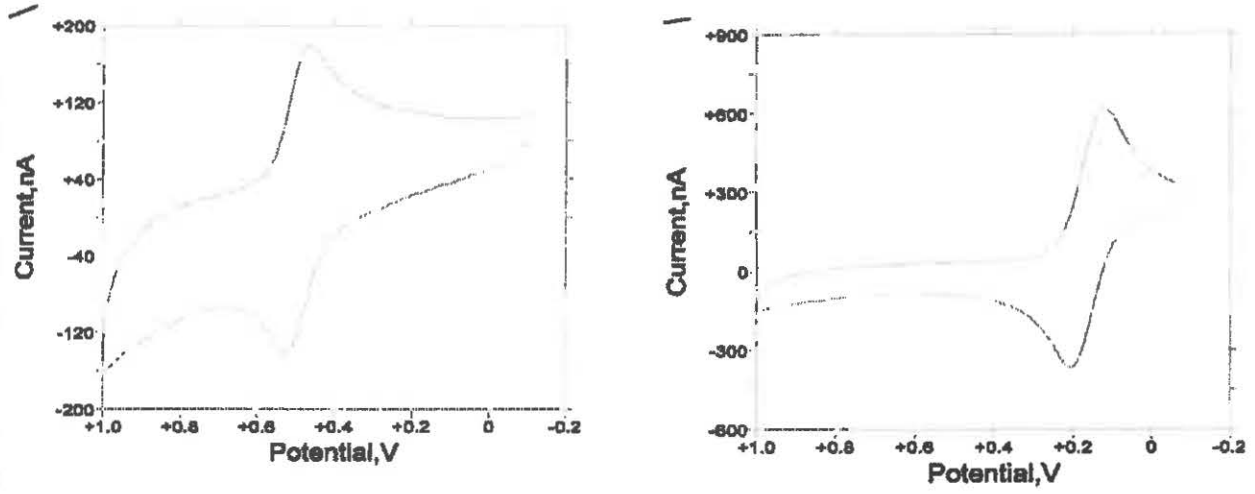

cis-[Ru(Phterpy)(HPB)(H_2O)](PF_6)$_2$·2H_2O **(2)**

trans-[Ru(Phterpy)(HPB)(H_2O)](PF_6)·2H_2O

Figure 12. Cyclic voltammograms of two aqua isomers, [Ru(Phterpy)(HPB)(H_2O)](PF_6).

3.2.3. Time-lapsed kinetics

In order to assess if each metal aqua complex interacts with CT-DNA, a time-lapsed kinetics experiment was performed. The spectrum of complex **1** in phosphate buffer (pH 7.0) with CT-DNA is shown in **Figure 13.** From previous UV-Vis spectroscopic experiments, the addition of the aqua ligand to the metal complex resulted in the formation of a band in the visible region (~750 nm) of the spectrum (**Figure 11**). As to be expected, **Figure 13** features the characteristic aqua absorption band in the visible region at 734 nm.

The experimental conditions involved following the reaction between the metal aqua complex and CT-DNA with time. As the reaction progressed, the absorption band at 734 nm decreased. Because there were only two components in the reaction cuvette, the decrease in absorbance gestured to the fact that there was some type of interaction occurring between the metal complex and CT-DNA. Note that the metal complex has a relatively high degree of stability and thus degradation of the complex is unlikely to account for the observed decrease in

absorbance. It is probable however that because aqua ligands are reported to be good leaving ligands, the CT-DNA is able to interact with the metal complex in such a way that results in the loss of the aqua ligand and, in turn, triggers a reduction in the absorbance of the solution.[31]

Similar time-lapsed kinetics spectra were obtained for complexes **2** and **3**, and it was decided that further experiments ought to be carried out in order to clarify the interaction between the metal aqua complexes and CT-DNA.

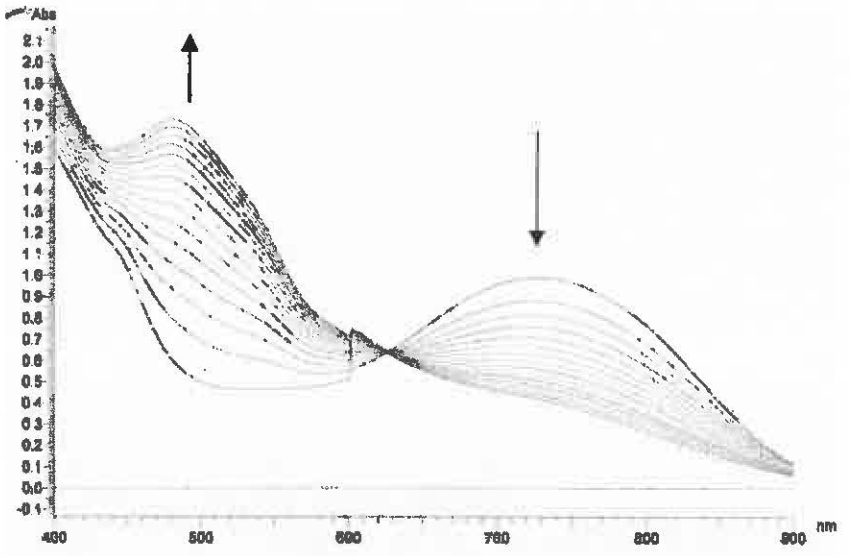

Figure 13. Time-lapsed kinetics spectra of complex **1** (0.25 mL, 6.645 X 10^{-4} M) and CT-DNA (0.75 mL, 2.588 X 10^{-4} M) measured in phosphate buffer (pH 7.0). Scans were recorded overnight in ninety minute intervals at 37 °C. The arrows show how the absorbance changes with time. Similar spectra were obtained for complexes **2** and **3**.

In order to quantitatively determine the rate of interaction between the metal aqua complex and CT-DNA, the change in absorbance at 734 nm was analyzed. Assuming that the reaction was pseudo-first order under the experimental conditions, a plot of $\ln(A_t - A_{inf})$ v. time (s) was used to describe the kinetics (**Graph 1**). The plot was expected to be linear with a slope of $-k_{obs}$,

where A_t was the absorbance at time t, A_{inf} was the absorbance at infinite time and k was the observed pseudo-first order rate constant.

As highlighted in **Table 3**, the observed rate constants follow the order of complex **2** > **1** > **3**. The addition of the electron donating phenyl group (complex **2**) does appear to positively enhance the rate of reaction between the complex and DNA; complex **2** has a higher observed rate constant than the unsubstituted terpyridine complex **1**. However if the trend for the observed rate constants were to be based solely on electronic effects, we would expect that the addition of an even stronger electron donating tolyl group (complex **3**) would have the highest observed rate constant. Surprisingly, complex **3** has the smallest observed rate constant. We propose that the addition of the methyl group (complex **3**) is causing unfavorable steric problems that hinders the interaction between the complex and CT-DNA.

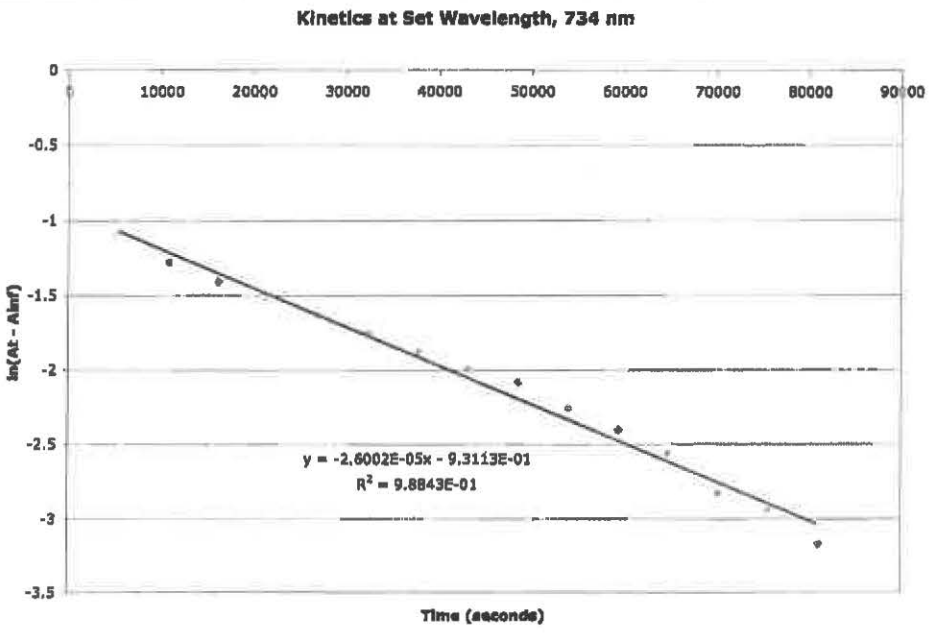

Graph 1. Analysis of time-lapsed kinetics data (λ = 734 nm). Plot of $\ln(A_t - A_{inf})$ v. time (s) for complex **1** where slope = $-k_{obs}$. Similar plots were obtained for complexes **2** and **3**.

Table 3. Summary of time-lapsed kinetics data, λ = 734 nm, derived from the plot of $\ln(A_t - A_{inf})$ v. time (s) where slope = $-k_{obs}$.	
Complex	Pseudo-first order rate constant, k_{obs} (s^{-1})
1	2.600×10^{-5}
2	3.473×10^{-5}
3	2.467×10^{-5}

3.2.4. X-ray crystal structure determination

The molecular structure of *trans*-[Ru(Phterpy)(HPB)Cl](PF_6) · $2H_2O$ has been established by single crystal x-ray diffraction. An ORTEP drawing of the complex is shown in **Figure 14.** Selected interatomic distances (Å) and angles (°) for the complex are reported in **Appendix 2.**

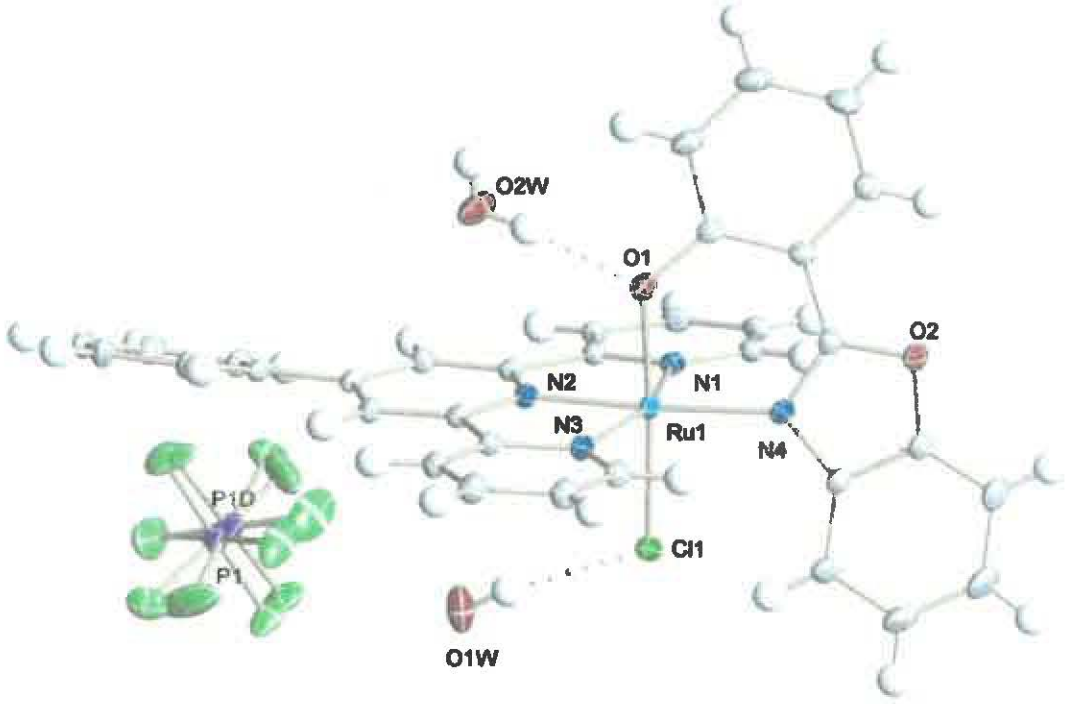

Figure 14. X-ray crystal structure determination of *trans*-[Ru(Phterpy)(HPB)Cl](PF_6)·$2H_2O$. Crystal data are given in **Appendix 1** and selected bond angles and bond lengths are listed in **Appendix 2.**

The crystal structure shows that the complex has a slightly distorted octahedral geometry around the ruthenium center and as a result, the Ru-N bond lengths of the Phenyl terpyridine ligand are not uniform. Despite the range from 1.9606 to 2.0882 Å, this was found to match well with Ru-N bond length values reported for other ruthenium terpyridine complexes.[36,46] The central Phenyl terpyridine ligand was also found to be bound trans to the imine nitrogen N(4), with an observed N(4)-Ru-N(2) angle of 177.01°. The other two terminal pyridine rings were found to be bound to the ruthenium center at angles N(2)-Ru-N(3) of 79.69° and N(1)-Ru-N(2) of 80.04°. Structural constraint is likely preventing the rings from binding to the ruthenium center at an ideal 90° angle.[47]

The Ru-Cl bond was found to be 2.3536 Å, while the bond length between the ruthenium and phenolic oxygen of the HPB ligand was found to be considerably shorter, 1.9646 Å. This Ru-O distance, however, was found to be comparable (1.9823 Å) to that of a similar ruthenium terpyridine complex, $[Ru(terpy)LCl]ClO_4$, which incorporated a phenolic Schiff base ligand, L.[47]

3.2.5. Absorption titration studies

Complex 1 was titrated with varying concentrations of CT-DNA and the change in the absorption spectrum at different [DNA] is shown in **Figure 15**. Upon increasing concentration of the CT-DNA, there is a clear decrease in absorbance. Additionally there is a shift of about 23 nm to longer wavelength. According to several authors, such an observation is indicative of an intercalation association between the complex and CT-DNA.[29,48,49,50]

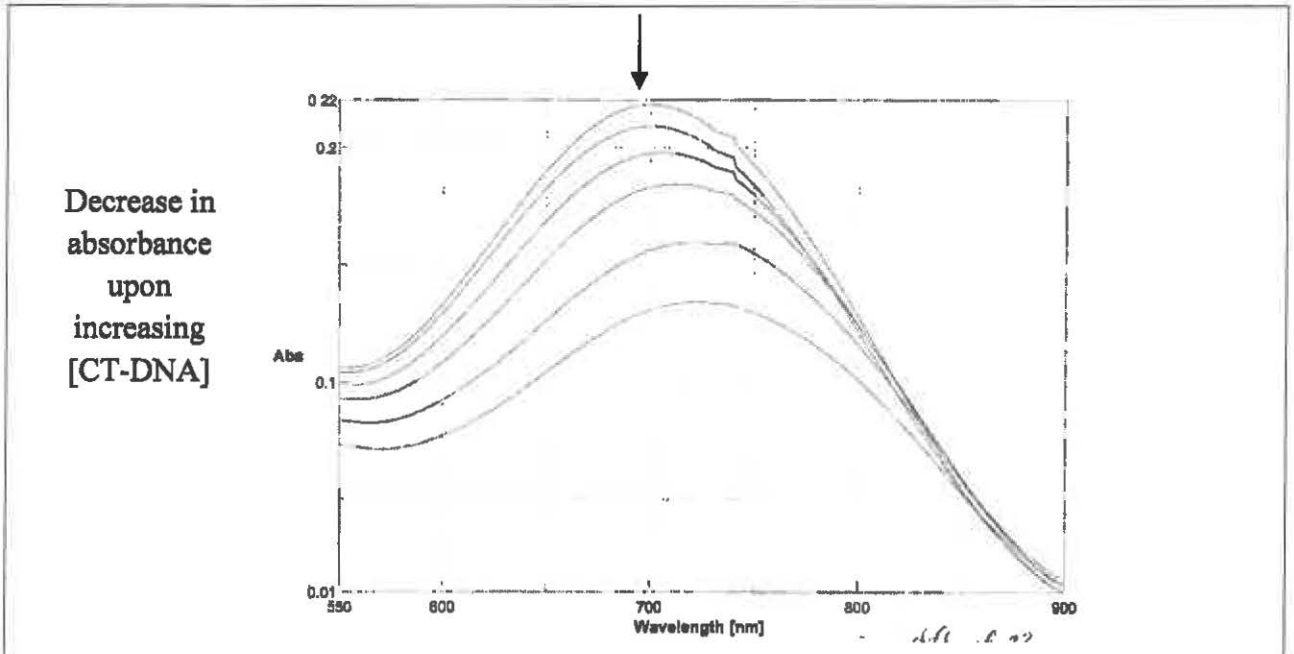

Figure 15. The overlay of the absorption titrations of **1** with CT-DNA ([DNA] = 0-100 μM) in phosphate buffer. Similar spectra have not been able to be obtained for complexes **2** and **3**.

When complexes **2** and **3** were titrated with varying concentrations of CT-DNA, the resulting spectra were quite erratic. Initially upon increasing the concentration of CT-DNA there was a decrease in absorbance, followed then by a drastic increase in absorbance (**Figure 16**). It is likely that experimental conditions are not ideal for these complexes.

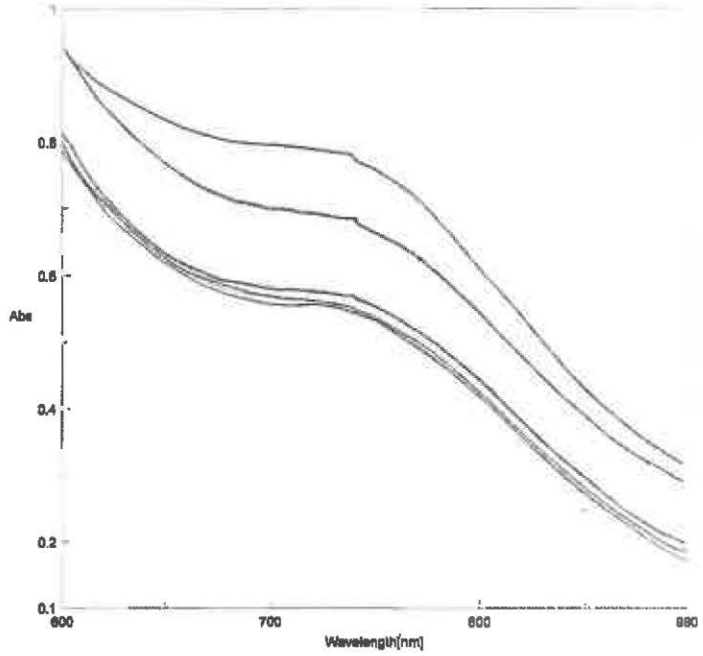

Figure 16. An absorption titration of **2** with CT-DNA ([DNA] = 0-100 μM) in phosphate buffer. The changes in absorbance do not follow any particular order upon increasing the concentration of DNA. Similar spectra were also obtained for complex **3**.

3.2.6. Competitive binding displacement with ethidium bromide (EB)

Although not a direct way to determine the binding mode between a metal complex and CT-DNA, per say, a competitive binding displacement assay is, nonetheless, a common experiment reported in the literature.[51,52] Its primary purpose is to measure the ability of a metal complex to affect the EB fluorescence intensity of an EB-DNA complex. Recall that although EB alone moderately emits, when it is combined with CT-DNA the emission intensity is greatly magnified. Therefore if a metal complex is found to have a high affinity for CT-DNA and is added to an EB-DNA solution, the metal will try to bind to DNA, potentially kicking out EB from the EB-DNA solution. If EB is displaced from the EB-DNA solution a decrease in the emission intensity will be observed. Note that this can only happen though if the metal complex

binds much more strongly to the CT-DNA than EB does. In other words, this experiment enables one to determine the extent at which the metal complex can competitively kick out EB bound to CT-DNA.

As was expected, upon adding complex **1** (0-300 μM) to CT-DNA pretreated with EB ([CT-DNA]/[EB] = 5) the emission intensity of the DNA-bound EB solution ($\lambda_{ex,}$ 537 nm) decreased (**Figure 17**). Similar spectra were also obtained for complexes **2** and **3**. The clear decrease in emission intensity upon addition of the complex suggested that metal complex efficiently competes with EB for binding positions on the CT-DNA. As proposed by other research teams, the decrease in emission intensity may be attributed to the complexes' ability to displace EB that has intercalated itself in between the base pairs of the DNA structure.[21,53]

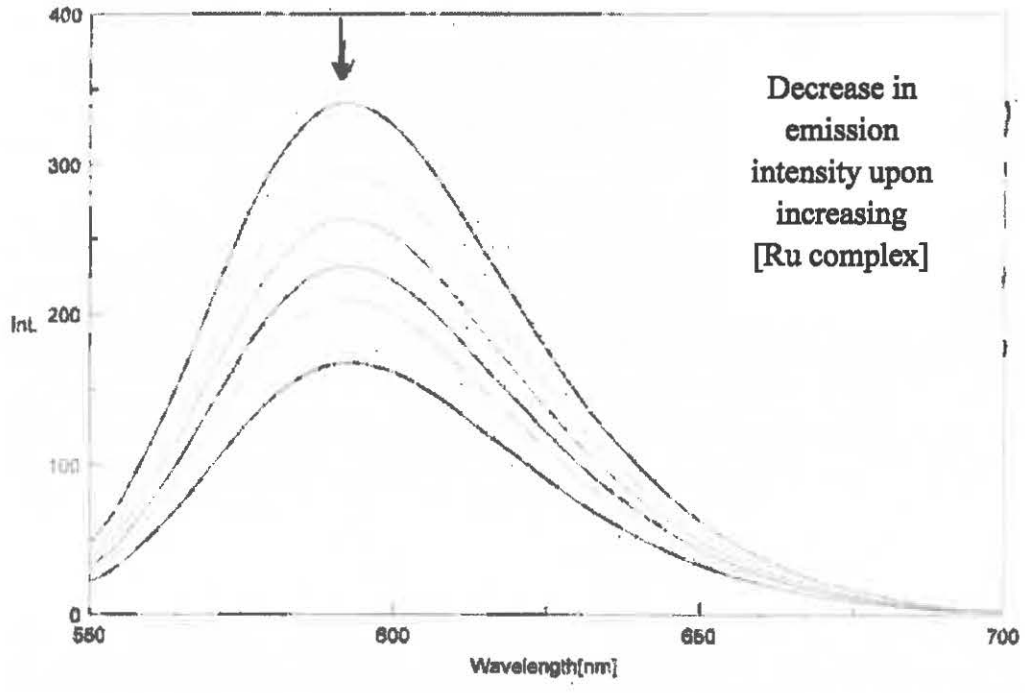

Figure 17. The overlay of the emission spectra of EB bound to DNA in the presence of complex **1**. [CT-DNA]/[EB] = 5; [Ru] = 0-300 μM. The arrow shows the change in emission intensity upon increasing concentration of the metal complex. Similar spectra were obtained for complexes **2** and **3**.

In order to further analyze the emission intensity spectrum, the Stern-Volmer equation (1) was used to derive a quenching plot, I_o/I v. [Ru]/[DNA] (**Graph 2**). From the slope, $K_{sv} = 0.482$ for complex **1** which was found to be higher than **2** ($K_{sv} = 0.401$) and **3** ($K_{sv} = 0.237$), measured all under the same conditions (**Table 4**). Based on the relative order of quenching constants (**1** > **2** > **3**) it is proposed that the addition of an electron donating substituent does not enhance the complexes' ability to quench fluorescence.

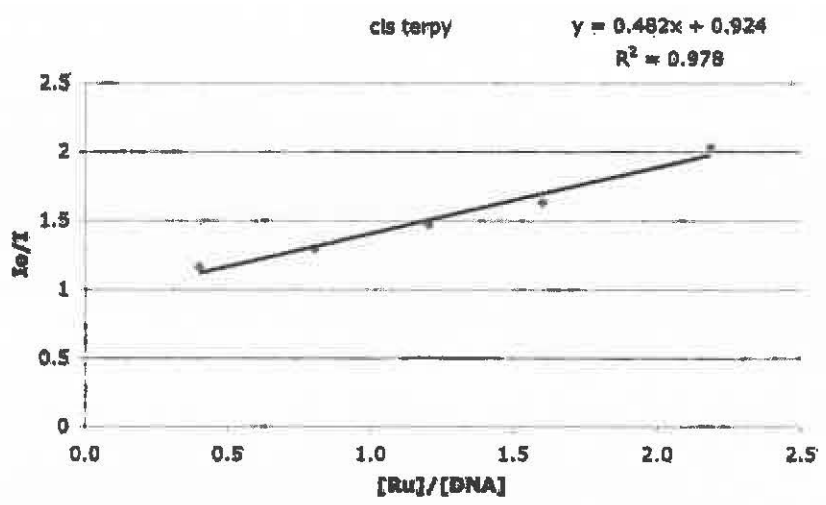

Graph 2. Analysis of emission spectral data. Plot of I_o/I v. [Ru]/[DNA] for complex **1** where slope = Stern-Volmer quenching constant, K_{sv}.

Table 4. Summary of competitive DNA binding study. Data derived from the plot of I_o/I v. [Ru]/[DNA] where slope = the Stern-Volmer quenching constant, K_{sv}.

Complex	K_{sv} from Stern-Volmer plot
1	0.482
2	0.401
3	0.237

3.2.7. DNA cleavage

Agarose gel electrophoresis is a standard method used to study the structural effects of drug-DNA binding. Under the influence of an electric field, this technique fractionates macromolecules on the basis of their movement through a gel.. Thus the size and charge of the macromolecule will greatly influence movement through the media. Small molecules are expected to progress further through the agarose matrix and with a faster rate of migration, while larger molecules will have a slower rate of migration. Therefore if a metal complex binds to a DNA molecule and the interaction induces a change in the mass, charge and / or tertiary structure of the DNA molecule, the migration of the DNA through the gel will be affected.

It is important to consider as well that DNA has three common forms: superhelical circular (form I); nicked circular (form II) and linear (form III).[54] The various forms of the DNA will migrate at different rates through the gel; linear form III typically has the slowest migration rate while supercoiled form I migrates the fastest. Because the gel can be visualized under UV light, any changes in the electrophoretic mobility of the DNA can be clearly assessed.

The interaction of complexes **1-3** with closed, superhelical plasmid pUC18 DNA was monitored using agarose gel electrophoresis. The complexes were incubated with DNA for one hour and then subjected to gel electrophoresis for ninety minutes at 60 V.

Many problems arose with this experiment. Gel preparation proved to be problematic. It was necessary for each gel to be made, however often times gels were prepared several days in advance and stored covered in buffer in the refrigerator. When the samples were ready to be analyzed the pre-made gel was removed from the refrigerator, samples were loaded into the wells, an electric field was applied and after a period of time the gel was visualized under UV light.

The reader will note that the sample gel image, as shown in **Figure 18**, has many white specks throughout. This contamination, which was often seen during beginning trials, detracts from the overall quality of the gel and is likely due to the fact that the agarose was not fully dissolved in the TAE buffer. Although the agarose and buffer solution were heated in the microwave for at least a minute, it is likely that the solution was poured into the loading apparatus before it was uniform in composition. As a result, any bands that might have been able to be visualized were compromised by the presence of undissolved agarose particles. The fact that the gels were made several days in advance also did not help the situation and it was decided that all gels should be meticulously prepared the day of analysis.

Figure 18. Sample gel image highlighting several problems 1) white specks throughout and 2) smearing in each lane with no clear bands in sample lanes A through E. Note that lane F corresponds to a 100 base pair marker.

Figure 18 highlights another problem often encountered: smearing in the sample lanes (note that the problem is more visible in the actual photograph as opposed to the scanned image included in this report). Although lanes A through E were loaded with a solution containing the metal complex, plasmid DNA and 6X loading dye, the only visualized bands were those from the base pair marker in lane F. Because the samples were loaded properly into the gel - as

determined by the visualization of the bands in lane F - the problem was thought to be due to the plasmid DNA concentration being too dilute.

It is probable as well that because the sample volume for each lane was so small, not all the materials were transferred into the loading wells. For instance, if some of the DNA sample was accidently loaded onto the side of the eppendorf tube, as opposed to the very bottom, it is likely that the DNA and metal complex would not be able to completely interact during the incubation period. Additionally we run the risk of not fully transferring the entire sample into the well. Thus it was beneficial to centrifuge each sample prior to incubation, and if necessary, prior to loading, to ensure that all components were properly transferred into the well.

By and large the agarose gel electrophoresis experiment was met with some success when the concentration of the DNA was increased relative to the metal complex concentration. As highlighted in **Figure 19**, bands were able to be visualized when the concentration of the plasmid DNA was increased relative to metal complex **1**. Although the presence of bands in the sample lanes is encouraging, further analysis revealed that it was unlikely that our metal complex interacted with the DNA. Note that lane F corresponds to a control sample which was incubated under identical experimental conditions, albeit containing only plasmid DNA - no metal complex. The reader is directed to also consider how the location of the bands in sample lanes A, B and D match up exactly with the bands in control lane F. (Lack of bands in sample lanes C and E are likely due to an operator loading error.) As stated earlier, we would expect that should the metal complex have an interaction with the DNA, a change will be induced in the DNA structure and thus the migration of the metal-DNA sample through the agarose matrix should differ from the migration of the DNA sample. In other words, because the electrophoretic

mobility pattern of the metal-DNA sample matches well with the mobility pattern of the control lane, there is no evidence of an interaction between the metal complex and the plasmid DNA.

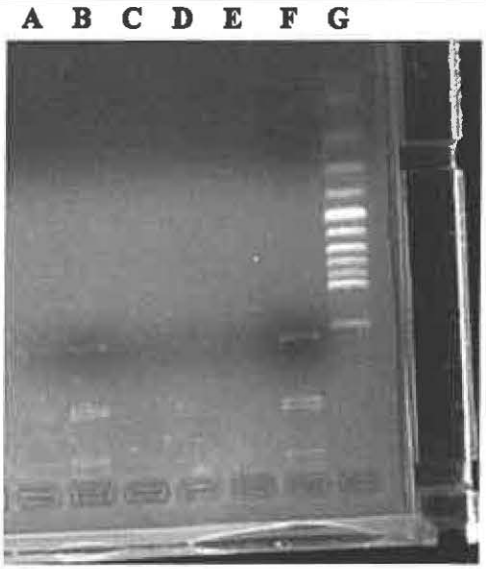

Figure 19. Sample gel image of plasmid DNA and increasing concentrations of complex **1** loaded from the right to the left. Lane G: 100 base pair marker. Lane F: control sample with only plasmid DNA, which was incubated under identical conditions. Lane E: least concentrated metal complex added to plasmid DNA. Lane A: most concentrated metal complex added to the plasmid DNA. Similar gels with clear band formation have not been obtained for complexes **2** and **3**.

Although the visualization of bands has been obtained for experiments using complex **1** and plasmid DNA, similar results have not been obtained using complexes **2** or **3**. It should be noted that this experiment is extremely sensitive to various experimental conditions, including, but not limited to, sample concentrations, sample incubation period, run time on the gel and the voltage applied to the gel. It is probable that no bands have been visualized for the other metal complexes with added substituents because experimental conditions are not optimal.

For purposes of comparison, consider the gel electrophoretic mobility pattern of pBR322 plasmid DNA with palladium and platinum metal complexes as reported by Ruiz *et al.* (**Figure 20**).[55] Lane 1 served as their DNA control and after visualization of the gel under UV light, they

noted the complexes ability to decrease the mobility of the DNA. The authors proposed that their complex had a direct impact on the tertiary structure of the DNA, inducing a change in both the open form (OC) and the covalently closed circular form (CCC) of plasmid DNA.

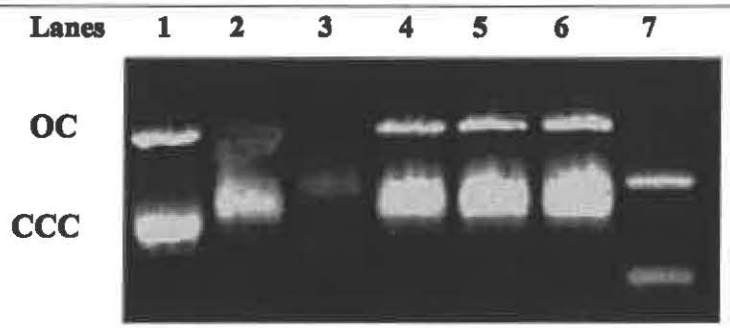

Figure 20. Agarose gel electrophoretic mobility pattern of plasmid DNA with various palladium and platinum metal complexes. Lane 1: plasmid DNA control. Sample lanes 2-7: plasmid DNA with various metal complexes. OC = open form of plasmid DNA, CCC = covalently closed circular form of plasmid DNA. Figure adopted from results published by Ruiz and co-workers.[55]

4. Summary of findings

4.1. Conclusion

Three novel ruthenium terpyridine complexes with the formula *cis*-[Ru(Terpy)(HPB)(OH_2)](PF_6) **1**, *cis*-[Ru(Phterpy)(HPB)(OH_2)](PF_6) **2** and *cis*-[Ru(Tterpy)(HPB)(OH_2)](PF_6) **3** have been synthesized and characterized by various spectroscopic means.

In order to evaluate the ability of the complex to interact with CT-DNA, absorption spectroscopy experiments as well as time-lapsed kinetics and competitive binding displacement assays with ethidium bromide were performed. In order to further evaluate the interaction of the metal complexes with plasmid DNA, agarose gel electrophoresis was performed and results obtained for complex **1** suggested that there was no interaction between the complex and the DNA. It might be interesting to adjust the incubation period of the complex and DNA from one

hour to fourteen hours, as suggested by Desphande and co-workers. They also report positive gel results with using a wider range of metal complex concentrations (10-70 uM).[42]

4.2. Future Work

For the immediate future, effort should be directed to learn how to harvest plasmid DNA. "Kits" available in the biology department enable the competent scientist to avoid buying plasmid DNA through commercial sources, but instead, to make it themselves. Because this reagent is costly it puts a lot of pressure to ensure that every experiment which uses the DNA yields meaningful results. Learning how to harvest the source in excess would allow for greater freedom to vary experimental conditions.

- Correct absorption titration for other complexes **2** and **3**
    - As proposed by Holmin *et al.* a more intense concentration difference between the metal complex and the DNA might yield better results.[25] For example, Ru 20 uM; CT-DNA 0-280 uM.
- Work out problems with gel electrophoresis
    - Try longer incubation (maybe 24 hours); add H_2O_2 prior to incubation period
    - Higgins and co-workers obtained positive results when they varied the concentration of the DNA, not the metal complex.[53] Other than this minor adaption the experimental conditions between our work and theirs were very similar.

It would be interesting to explore the biological effects of the metal complexes with various biomolecules. Collaboration with the biology department may allow for the cytotoxicity activity

of our metal complexes toward cisplatin resistant cancer cells to be evaluated. It would be especially interesting to compare the complexes' calculated resistance factors (RF) to that of cisplatin (RF = 5.61).[56]

5. Appendix

Appendix 1. Crystal data and structure refinement for *trans*-[Ru(Phterpy)(HPB)Cl](PF$_6$)·2H$_2$O	
Identification code	ha13_0m
Empirical formula	$C_{34}H_{25.41}ClF_6N_4O_{3.21}PRu$
Formula weight	822.76
Temperature (K)	100(2)
Wavelength (Å)	0.71073
Crystal system	Triclinic
Space group	P-1
Unit cell dimensions	
a (Å)	10.1967(3)
b (Å)	11.9503(4)
c (Å)	14.1934(5)
α (°)	112.8086(4)
β (°)	91.7830(4)
γ (°)	95.5838(4)
V (A^3)	1582.24(9)
Z	2
D_{calc} (Mg m^{-3})	1.727
Absorption coefficient (mm^{-1})	0.711
F(OOO)	826
Crystal size (mm^3)	0.47 x 0.43 x 0.23
θ range for data collection (°)	1.90 to 29.57
Index ranges	$-14 \leq h \leq 14, -16 \leq k \leq 16, -19 \leq l \leq 19$
Reflections collected	35319
Independent reflections	8852 [R_{int} = 0.0153]
Completeness to θ = 29.57° (%)	99.7
Absorption correction	Semi-empirical from equivalents
Max. and min. transmission	0.8541 and 0.7319
Refinement method	Full-matrix least squares on F^2
Data / restraints / parameters	8852 / 282 / 537
Goodness-of-fit on F^2	1.030
Final R indices [$I > 2\sigma(I)$]	R_1 = 0.0229, wR_2 = 0.0599
R indices (all data)	R_1 = 0.0241, wR_2 = 0.0609
Largest difference peak and hole (e.Å^{-3})	1.569 and -0.387

Appendix 2. Selected interatomic distances (Å) and angles (°) for complex *trans*-[Ru(Phterpy)(HPB)Cl](PF$_6$)·2H$_2$0	
Bond Lengths, Å	
Ru(1)-N(2)	1.9606(11)
Ru(1)-O(1)	1.9646(10)
Ru(1)-N(3)	2.0542(11)
Ru(1)-N(4)	2.0881(11)
Ru(1)-N(1)	2.0882(11)
Ru(1)-Cl(1)	2.3536(3)
Bond Angles, °	
N(2)-Ru(1)-O(1)	88.19(4)
N(2)-Ru(1)-N(3)	79.69(4)
O(1)-Ru(1)-N(3)	90.64(4)
N(2)-Ru(1)-N(4)	177.01(4)
O(1)-Ru(1)-N(4)	88.83(4)
N(3)-Ru(1)-N(4)	100.29(4)
N(2)-Ru(1)-N(1)	80.09(4)
O(1)-Ru(1)-N(1)	89.80(4)
N(3)-Ru(1)-N(1)	159.75(4)
N(4)-Ru(1)-N(1)	99.97(4)
N(2)-Ru(1)-Cl(1)	87.80(3)
O(1)-Ru(1)-Cl(1)	175.70(3)
N(3)-Ru(1)-Cl(1)	90.17(3)
N(4)-Ru(1)-Cl(1)	95.19(3)
N(1)-Ru(1)-Cl(1)	87.98(3)

6. References

[1] Rosenberg, B.; VanCamp, L.; Trosko, J.E.; Mansour, V.H. Platinum Compounds: a New Class of Potent Antitumour Agents. *Nature.* **1969**, *222*, 385-386.

[2] O'Dwyer, P.; Stevenson, J.; Johnson, S. Clinical Status of Cisplatin, Carboplatin and Other Platinum-Based Antitumor Drugs. In *Cisplatin: Chemistry and Biochemistry of a Leading Anticancer Drug;* Bernhard, L., Ed.; Verlag Helvetica Chimica Acta: Switzerland, 1999; pp 31-70.

[3]Thompson, A.J.; Williams, R.J.P.; Reslova, S. The chemistry of complexes related to *cis*-$Pt(NH_3)_2Cl_2$: an anti-tumor drug. *Structure and Bonding.* **1972**, *11*, 1-42.

[4] Natile, G.; Cannito, F. Platinum Drugs, Nucleotides and DNA: The Role of Interligand Interactions. In *Metal Complex-DNA Interactions;* Hadjiliadis, N., Sletten, E., Eds.; Wiley: United Kingdom, 2009; pp 135-173.

[5] Reedijk, J.; Lohman, P.H.M. Cisplatin: synthesis, antitumor activity and mechanism of action. *Pharmaceutisch Weekblad Scientific Edition.* **1985**, *7*, 173-180.

[6]Richards, A.D.; Rodger, A. Synthetic metallomolecules as agents for the control of DNA. *Chemical Society Review.* **2007**, *36*, 471-483.

[7] Reedijk, J.; Teuben, J.M. Platinum-Sulfur Interactions Involved in Antitumor Drugs, Rescue Agents and Biomolecules. In *Cisplatin: Chemistry and Biochemistry of a Leading Anticancer Drug;* Bernhard, L., Ed.; Verlag Helvetica Chimica Acta: Switzerland, 1999; pp 339-362.

[8] Siddik, Z.H. Cisplatin Resistance. In *Cancer Drug Resistance;* Teicher, B.A., Ed.; Humana Press: New Jersey, 2006; pp 283-308.

[9] Sherman, S.E.; Lippard, S.J. Structural Aspects of Platinum Anticancer Drug Interactions with DNA. *Chemical Reviews.* **1987**, *87*, 1153-1181.

[10] Jamesdaniel, S.; Ding, D.; Kermany, M.H.; Davidson, B.A.; Knight, P.R.; Salvi, R.; Coling, D.E. Proteomic Analysis of the Balance between Survival and Cell Death Responses in Cisplatin-Mediated Ototoxity. *Journal of Proteome Research.* **2008**, *7*, 3516-3524.

[11] Buchanan, R.L.; Gralla, J.D. Cisplatin Resistance and Mechanism in a Viral Test System. *Biochemistry.* **1990**, *29*, 3436-3442.

[12] Tsao, A.S.; Stewart, D.L. Collateral Damage Associated with Chemotherapy. In *Medical Care of Cancer Patients;* Yeung, S.; Escalante, C.; Gagel, R., Eds.; BC Decker: Shelton, 2009; pp 18-32.

[13] Galanski, M.; Jakupec, M.A.; Keppler, B.K. Update of the preclinical situation of anticancer platinum complexes: novel design strategies and innovative analytical approaches. *Current Medicinal Chemistry.* **2005**, *12*, 2075-2094.

[14] Aebi, S.; Kurdi-Haidar, B.; Gordon, R.; Cenni, B.; Zheng, H.; Fink, D.; Christen, R.D.; Boland, C.R.; Koi, M.; Fishel, R.; Howell, S.B. Loss of DNA Mismatch Repair in Acquired Resistance to Cisplatin. *Cancer Research.* **1996**, *56*, 3087-3090.

[15] Novakova, O.; Kasparkova, J.; Vrana, O.; van Vliet, P.M.; Reedijk, J.; Brabec, V. Correlation between Cytotoxicity and DNA Binding of Polypyridyl Ruthenium Complexes. *Biochemistry*. **1995**, *34*, 12369-12378.

[16] Velders, A.H.; Kooijman, H.; Spek, A.L.; Haasnoot, J.G.; de Vos, D.; Reedijk, J. Strong Differences in the in Vitro Cytotoxicity of Three Isomeric Dichlorobis(2-phenylazopyridine)ruthenium(II) Complexes. *Inorganic Chemistry*. **2000**, *39*, 2966-2967.

[17] Morris, R.E.; Aird, R.E.; del Socorro Murdoch, P.; Chen, M.; Cummings, J.; Hughes, N.D.; Parsons, S.; Parkin, A.; Boyd, G.; Jodrell, D.I.; Sadler, P.J. Inhibition of Cancer Cell Growth by Ruthenium(II) Arene Complexes. *Journal of Medicinal Chemistry*. **2001**, *44*, 3616-3621.

[18] Sava, G.; Alessio, E.; Bergamo, A.; Mestroni, G. Sulfoxide ruthenium complexes. *Topics in Biological Inorganic Chemistry*. **1999**, *1*, 143-169.

[19] Pieper, T.; Borsky, K.; Keppler, B.K. Non-platinum antitumor compounds. *Topics in Biological Inorganic Chemistry*. **1999**, *1*, 171-199.

[20] Sadler, P.J.; Muncie, C.; Shipman, M.A. Metals in Medicine. In *Biological Inorganic Chemistry: Structure and Reactivity;* Bertini, I.; Gray; Stiefel; Valentine, Eds.; University Science: USA, 2007; pp 95-136.

[21] Tan, C.; Liu, J.; Chen, L.; Shi, S..; Ji, L. Synthesis, structural characteristics, DNA binding properties and cytotoxicity studies of a series of Ru(III) complexes. *Journal of Inorganic Biochemistry*. **2008**, *102*, 1644-1653.

[22] Sadler, P.J.; Muncie, C.; Shipman, M.A. Metals in Medicine. In *Ruthenium in Organic Synthesis;* Murahashi, S., Ed.; Wiley VCH: Weinheim, 2004; pp 95-136.

[23]Gao, F.; Chen, X.; Wang, J.; Chen, Y.; Chao, H.; Ji, L. In Vitro Transcription Inhibition by Ruthenium(II) Polypyridyl Complexes with Electropositive Ancillary Ligands. *Inorganic Chemistry*. **2009**, *48*, 5599-5601.

[24] Rani-Beeram, S.; Meyer, K.; McCrate, A.; Hong, Y.; Nielsen, M.; Swavey, S. A Fluorinated Ruthenium Porphyrin as a Potential Photodynamic Therapy Agent. *Inorganic Chemistry*. **2008**, *47*, 11278-11283.

[25] Holmin, R.E.; Stemp, E.D.A.; Barton, J.K. $Ru(phen)_2dppz^{2+}$ Luminescence: Dependence on DNA Sequences and Groove-Binding Agents. *Inorganic Chemistry*. **1998**, *37*, 29-34.

[26] Miessler, G.L.; Tarr, D.A. *Inorganic Chemistry, 4th Edition*; Prentice Hall: 2011; pp 483-488.

[27] Gao, F.; Chao, H.; Wang, J.; Yuan, Y.; Sun, B.; Wei, Y.; Peng, B.; Ji, L. Targeting topoisomerase II with the chiral DNA-intercalating ruthenium(II) polypyridyl complexes. *Journal of Biological Inorganic Chemistry*. **2007**, *12*, 1015-1027.

[28] Tan, L.F.; Wang, F.; Chao, H.; Zhang, S.; Fei, J.J.; Ji, L.N. DNA Interactions of the Functionalized (Mixed Polypyridine)Ruthenium(II) Complex $[Ru(bpy)_2(dppz\text{-}11\text{-}CO_2Me)]^{2+}$. *Helvetica Chimica Acta*. **2008**, *91*, 1251-1260.

[29] Ambroise, A.; Maiya, B.G. Ruthenium(II) Complexes of 6,7-Dicyanodipyridoquinoxaline: Synthesis, Luminescence Studies, and DNA Interaction. *Inorganic Chemistry*. **2000**, *39*, 4264-4272.

[30] Narra, M.; Elliott, P.; Swavey, S. Synthesis, characterization and DNA interactions of 5,15-(4-pyridyl)-10,20-(pentafluorophenyl)porphyrin coordinated to two $[Ru(bipy)_2Cl]^+$ groups. *Inorganica Chimica Acta*. **2006**, *359*, 2256-2262.

[31] Grover, N.; Welch, T.W.; Fairley, T.A.; Cory, M.; Thorp, H.H. Covalent binding of Aquaruthenium complexes to DNA. *Inorganic Chemistry*. **1994**, *33*, 3544-3548.

[32] Pyle, A.M.; Rehmann, J.P.; Meshoyrer, R.; Kumar, C.V.; Turro, N.J.; Barton, J.K. Mixed-Ligand Complexes of Ruthenium(II): Factors Governing Binding to DNA. *Journal of the American Chemical Society*. **1989**, *111*, 3051-3058.

[33] Schubert, U.; Hofmeier, H.; Newkom, G.R. *Modern Terypyridine Chemistry*; Wiley VCH: 2006; pp 162.

[34] Marmur, J. A Procedure for the Isolation of Deoxyribonucleic Acid from Micro-Organisms. *Journal of Molecular Biology*. **1961**, *3*, 208-211.

[35] Reichmann, M.E.; Rice, S.A.; Thomas, C.A.; Doty, P. A Further Examination of the Molecular Weight and Size of Desoxypentose Nucleic Acid. *Journal of the American Chemical Society*. **1954**, *76*, 3047-3053.

[36] Claustro, I.; Abate, G.; Sanchez, E.; Acquaye, J.H. Synthesis, spectroscopic and electrochemical properties of ruthenium-2-(2'-hydroxyphenyl)-benzoxazole complexes. Crystal structure of [Ru(terpy)(HPB)Cl]. *Inorganica Chimica Acta*. **2003**, *342*, 29-36.

[37] *APEX 2*, version 2009.5-1, Bruker (2009), Bruker AXS Inc., Madison, Wisconsin, USA.

[38] *SAINT*, version V7.60A, Bruker (2009), Bruker AXS Inc., Madison, Wisconsin, USA.

[39] *SADABS*, version 2008/1, Bruker (2008), Bruker AXS Inc., Madison, Wisconsin, USA.

[40] *SHELXTL*, version 2008/4, Bruker (2008), Bruker AXS Inc., Madison, Wisconsin, USA.

[41] Tan, C.; Liu, J.; Li, H.; Zheng, W.; Shi, S.; Chen, L.; Ji L. Differences in structure, physiological stability, electrochemistry, cytotoxicity, DNA and protein binding properties between two Ru(III) complexes. *Journal of Inorganic Biochemistry*. **2008**, *102*, 347-358.

[42] Deshpande, M.S.; Kumbhar, A.A.; Kumbhar, A.S. Hydrolytic Cleavage of DNA by a Ruthenium(II) Polypyridyl Complex. *Inorganic Chemistry*. **2007**, *46*, 5450-5452.

[43] Gerli, A.; Reedijk, J.; Lakin, M.T.; Spek, A.L. Redox Properties and Electrocatalytiic Activity of the Oxo/Aqua System $[Ru(terpy)(bpz)(O)]^{2+}/[Ru(terpy)(bpz)(H_2O)]^{2+}$. *Inorganic Chemistry*. **1995**, *34*, 1836-1843.

[44] Hecker, C.R.; Fanwick, P.E.; McMilin, D.R. Evidence of Dissociative Photosubstitution Reactions of $[Ru(trpy)(bpy)(NCCH_3)]^{2+}$. *Inorganic Chemistry*. **1991**, *30*, 659-666.

[45] Balzani, V.; Juris, A.; Venturi, M. Luminescent and Redox-Active Polynuclear Transition Metal Complexes. *Chemical Reviews*. **1996**, *96*, 759-833.

[46] Mosher, P.J.; Yap, G.P.A.; Crutchley, R.J. Influence of the Inner Coordination Sphere on the Ru(III)-Cyanamido Ligand-to-Metal Charge Transfer Chromophore. *Inorganic Chemistry*. **2001**, *40*, 550-553.

[47] Mondal, B.; Chakraborty, S.; Munshi, P.; Walawalkar, M.G.; Lahiri, G.K. Ruthenium (II)/(III) terpyridine complexes incorporating imine functionalities. Synthesis, structure, spectroscopic and electrochemical properties. *Dalton Transactions*. **2000**, 2327-2335.

[48] Deng, H.; Cai, J.; Xu, H.; Zhang, H.; Ji, L-N. Ruthenium(II) complexes containing asymmetric ligands: synthesis, characterization, crystal structure and DNA-binding. *Dalton Transactions*. **2003**, 325-330.

[49] Liu, Y.J.; Zeng, C.H. Synthesis and DNA interaction studies of ruthenium(II) complexes with isatino[1,2-b]-1,4,8,9-tetraazatriphenylene as an intercalative ligand. *Transition Metal Chemistry*. **2009**, *34*, 455-462.

[50] Dey, S.; Sarkar, S.; Paul, H.; Zangrando, E.; Chattopadhyay, P. Copper(II) complex with tridentate N donor ligand: synthesis, crystal structure, reactivity and DNA binding study. *Polyhedron*. **2010**, *29*, 1583-1587.

[51] Mei, W-J.; Liu, J.; Chao, H.; Ji, L-N.; Li, A-X.; Liu, J-Z. DNA-binding and cleavage studies of a novel porphyrin ruthenium mixed complex [MPyTPP-Ru(pip)2Cl]$^{+}$. *Transition Metal Chemistry*. **2003**, *28*, 852-857.

[52] Chen, L.M.; Liu, J.; Chen, J.C.; Tan, C.P.; Shi, S. Synthesis, characterization, DNA-binding and spectral properties of complexes $[Ru(L)_4(dppz)]^{2+}$ (L=Im and MeIm). *Journal of Inorganic Biochemistry*. **2008**, *102*, 330-341.

[53] Higgins, S.L.H.; White, T.A.; Winkel, B.S.; Brewer, K. J. Redox, Spectroscopic, and Photophysical Properties of Ru-Pt Mixed-Metal Complexes Incorporating 4,7-Diphenyl-1,10-phenanthroline as Efficient DNA Binding and Photocleaving Agents. *Inorganic Chemistry*. **2011**, *50*, 463-470.

[54] Sambrook, J.; Russell, D.W. *Molecular cloning: a laboratory manual, volume 2*; Cold Spring Harbor Laboratory Press: 2001; p Protocol 1: Agarose Gel Electrophoresis, 5.5.

[55] Ruiz, J.; Lorenzo, J.; Vicente, C.; Lopez, G.; Lopez-de-Luzuriaga, J.M.; Monge, M.; Aviles, F.X.; Bautista, D.; Moreno, V.; Laguna, A. New Palladium(II) and Platinum(II) Complexes with 9-Aminoacridine: Structures, Luminescence, Theoretical Calculations, and Antitumor Activity. *Inorganic Chemistry*. **2008**, *47*, 6990-7001.

[56] Linares, F.; Galindo, M.A.; Galli, S.; Romero, M.A.; Navarro, J.A.R.; Barea, E. Tetranuclear Coordination Assemblies Based on Half-Sandwich Ruthenium(II) Complexes: Noncovalent Binding to DNA and Cytotoxicity. *Inorganic Chemistry*. **2009**, *48*, 7413-7420.